3.1 INTRODUCTION

The present chapter investigates the effect of build orientation on the microstructure and physical properties of maraging steel processed by Additive Manufacturing (AM) and conventional manufacturing (CM). AM plates were processed in orientations of 0°, 45°, and 90° and were given solution treatment and aging. The density, surface roughness, and microstructural characterization of all the samples were measured and compared with those of CM samples.

3.2 POWDER CHARACTERIZATION

3.2.1 Powder Morphology

The variation of the particle size distribution and morphology of gas-atomized maraging steel powder, the SEM analysis and histogram are shown in Fig.3.1. It can be concluded that almost fully spherical powder particles with a very little amount of satellite particles with size range of (14-40) µm, which is recommended for powder bed system (PBF), one of the potential AM techniques [120].

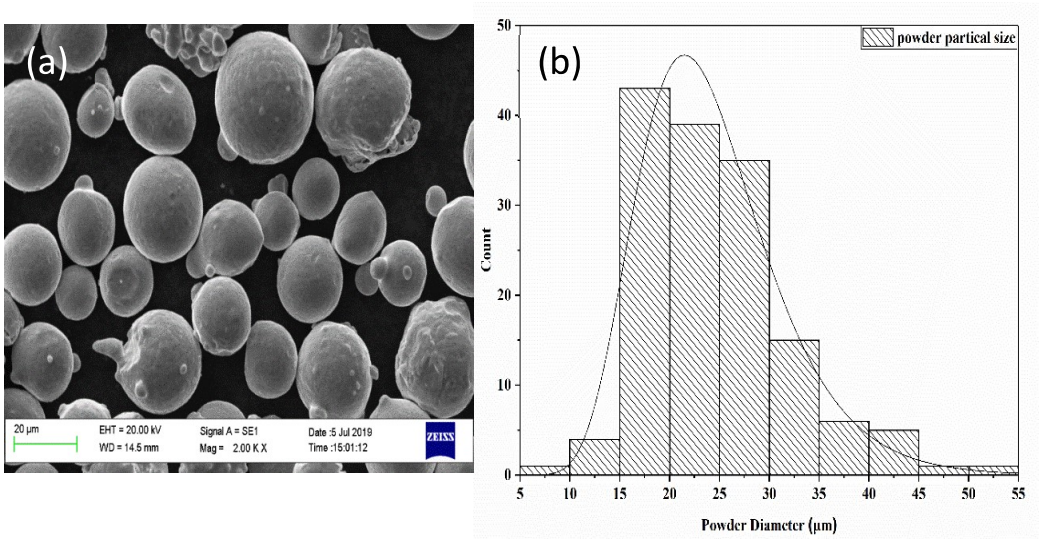

Fig. 3.1 (a) Morphology of M300 Powder particles and (b) Histogram showing powder size distribution.

Powders were mounted, polished, etched and analysed by Scanning Electron Microscopy (SEM). The cross-section of the single particle after polishing and etching is given in Fig. 3.2(a) which reveals dendritic structure, which is characteristic of gas atomized AM powder due to very high cooling rate during solidification. The EDS area scan of cross-section of AM powder in Fig.3.2(b) confirms that there is no loss of chemical constituents.

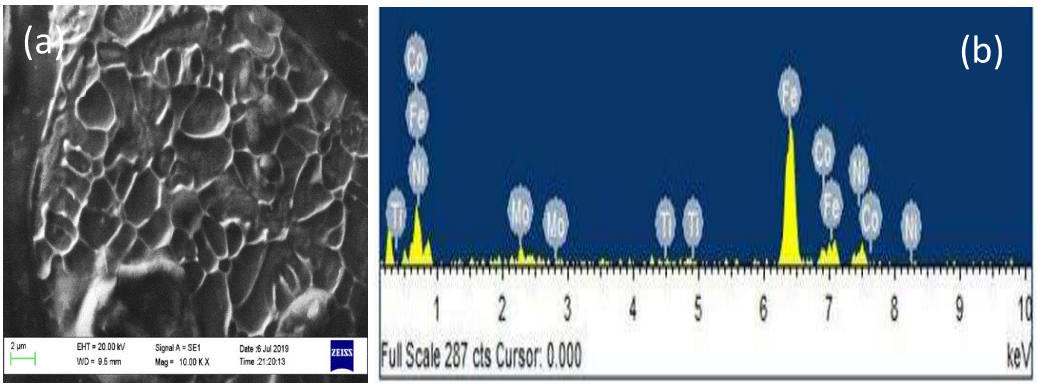

Fig.3.2 (a) Gas atomized single powder particle showing dendrites and (b) EDS analysis of powder.

3.2.2 Density and surface roughness

AM processed plates [Fig.2.1(c)] of size 55×55×5 mm^3 built in 0º, 45º and 90º orientations were tested for relative density and surface roughness. Values of surface roughness in different orientations of AM plates along with density are listed in Table 3.1. Results suggest that there was little variation in density with change in built orientation. AM plates in all orientations showed densities greater than 99.6% as compared to the density of conventional maraging steel (8.1g/cm^3). As-built (AB) AM samples in 45º orientation showed significantly higher surface roughness i.e., 6.3 µm than the values of samples built in 0º and 90º orientations, which are measured to be 3.5 µm and 3.4 µm respectively.

Table 3.1 Variation of surface roughness and density of as-built AM (additive manufactured) samples in different orientations.

Build Orientation	Surface Roughness (µm)			Density of AM plate (g/cm^3)
	R_a	R_q	R_z	
0° AM	3.5	4.3	16.7	8.09
45° AM	6.3	7.9	33.8	8.06
90° AM	3.4	4.3	18.8	8.08

3.3 MICROSTRUCTURAL CHARACTERIZATION

3.3.1 Microstructure of as-built (AB) and conventionally manufactured (CM) samples

Samples were printed in 0°, 45° and 90° build orientations with respect to base plate. Samples were not taken from the same build in different orientations. In additive manufacturing of metals, due to its unique processing strategy, two types of structures are revealed by optical microscopy i.e., meso- and micro-structure. In the present case [Fig. 3.3(a and c)], at lower magnification, laser tracks on top faces are visible (facing laser source in build chamber) mainly in 0° and 90° orientations of as-built AM samples. Series of ends of laser tracks are visible in samples built in 45° orientation [Fig. 3.3(b)]. Melt pool characteristics are visible in top, transverse and long transverse faces of the as-built AM samples represented as three faces of cube as shown in Fig. 3.3. Three consecutive stacked layers are visible in Figs. 3.3 (a) and (c). In 0° orientation, the starting point of laser tracks are clearly visible without any overlapping of parallel tracks that show the laser spot diameter measured to be approximately 79 µm. The overlapped width is also measured which shows 44% overlapped regions. In the transverse direction, the layer thickness is measured to be around 32 µm. Melt pool depth is observed as semi-elliptical in shape with depth size varying from 87 to 65 µm.

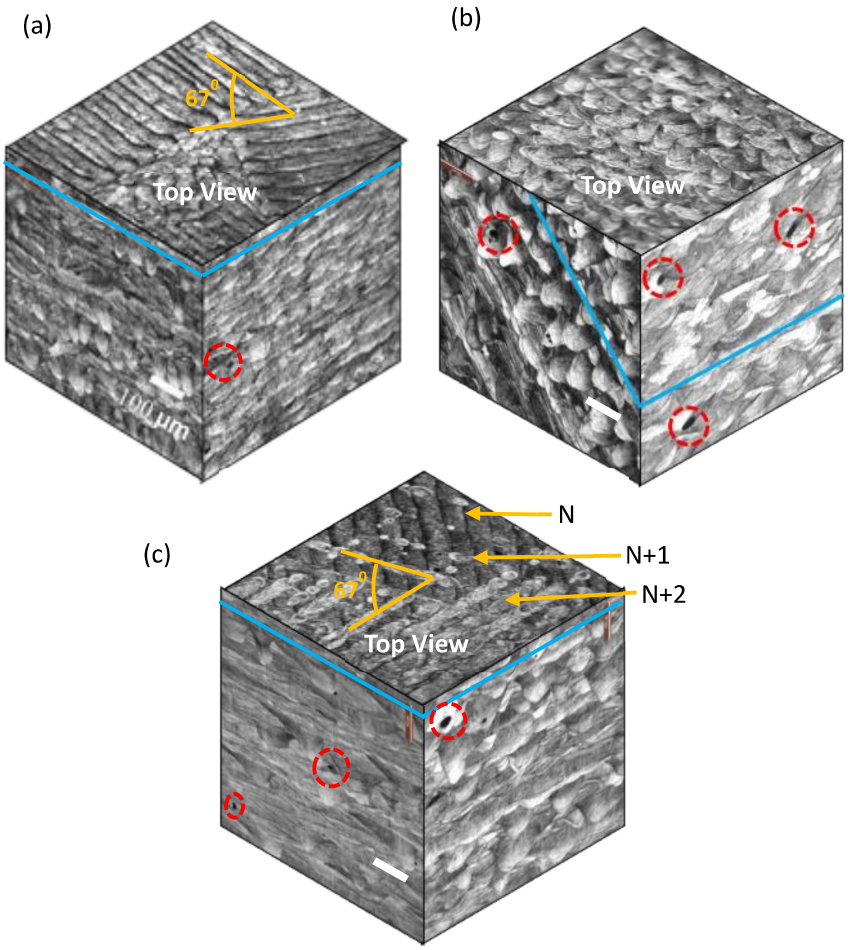

Fig. 3.3 Optical Micrographs of AB samples of M300 in (a) 0° orientation (b) 45° Orientation and (c) 90° orientations, showing hatch pattern and 67° inter layer rotation in top view and melt pool characteristics in transverse views. Blue colour line shows deposition layers, red circles show voids/pores. Also, N, N+1, N+2 successive deposited layers are shown by yellow arrows.

At higher magnification, cellular and columnar type microstructure can be seen. Mainly at the boundary of melt pool, columnar grains of length 4-8 µm and width 0.2-0.3 µm can be observed and at away from melt pool boundary, cellular grains of size 0.2-0.6 µm can be seen in AM samples as shown in Fig. 3.4 (a).

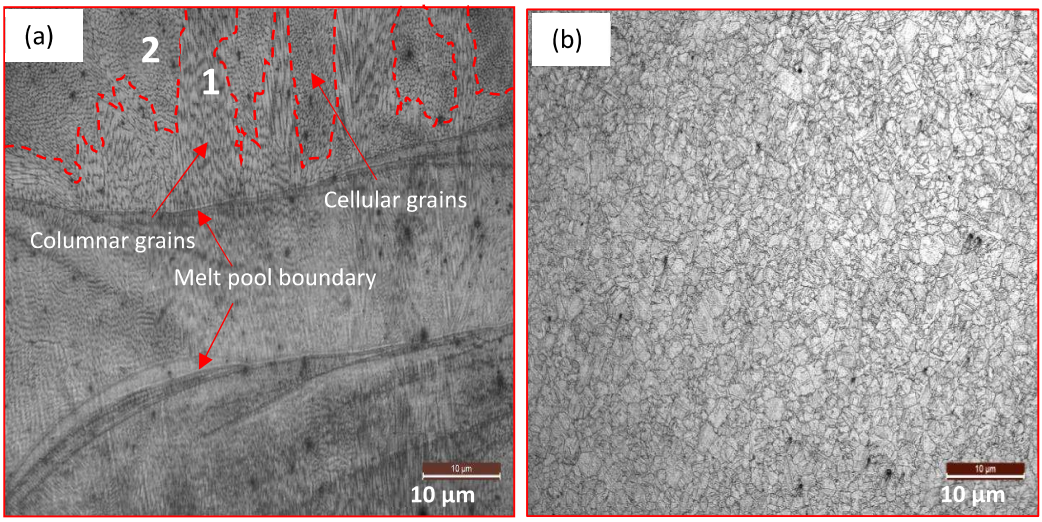

Fig. 3.4 Optical Micrographs of M300 steel: (a) Transverse section of AB sample in 0^{o} orientation showing columnar and cellular grains. Also marked as 1 and 2 (b) CM sample showing coarse equiaxed grains.

In conventionally fabricated (CM) samples, equiaxed grains can be seen as shown in Fig.3.4 (b). SEM micrograph of the as-built AM sample at lower magnification reveals melt pool boundaries as visualized in Fig. 3.5(a). At higher magnification, columnar and cellular grains can be seen as shown in Fig. 3.5(b) similar to that reported earlier [121, 122].

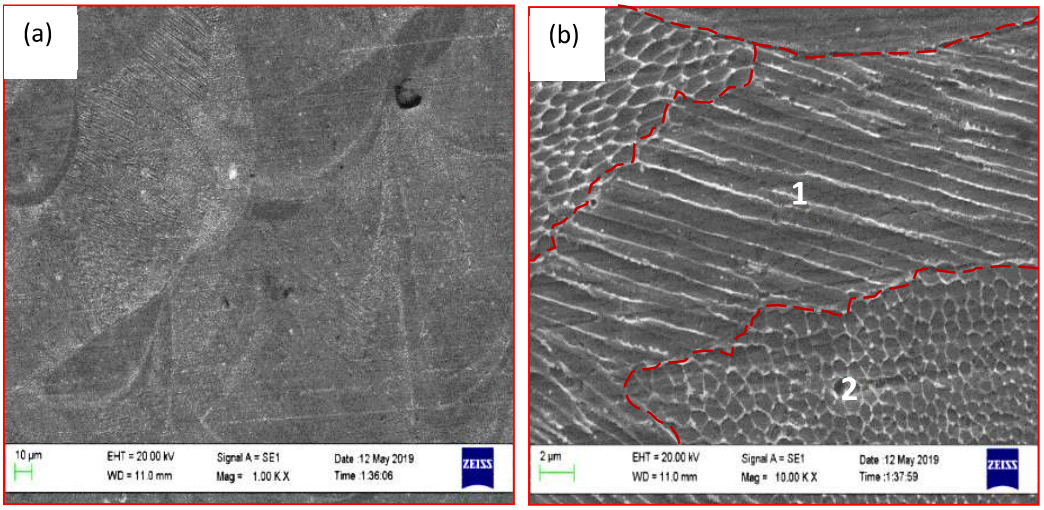

Fig. 3.5 SEM micrographs of transverse section of AM sample in 0^0 orientation showing: (a) melt pools and (b) magnified view of (a) showing columnar grains (marked as 1) and cellular grains (marked as 2).

X-ray diffraction analysis of M300 powder and as-built AM samples shows bcc phase with a small amount of austenite phase (*fcc*) as given in Fig. 3.6. The volume fraction of retained austenite was found to be 5% in the M300 powder. However, the volume fraction of retained austenite decreased in samples processed by AM and was found to be 2%, 3% and 2% retained austenite in 0^o, 45^o, and 90^o orientations respectively as shown in Table 3.2.

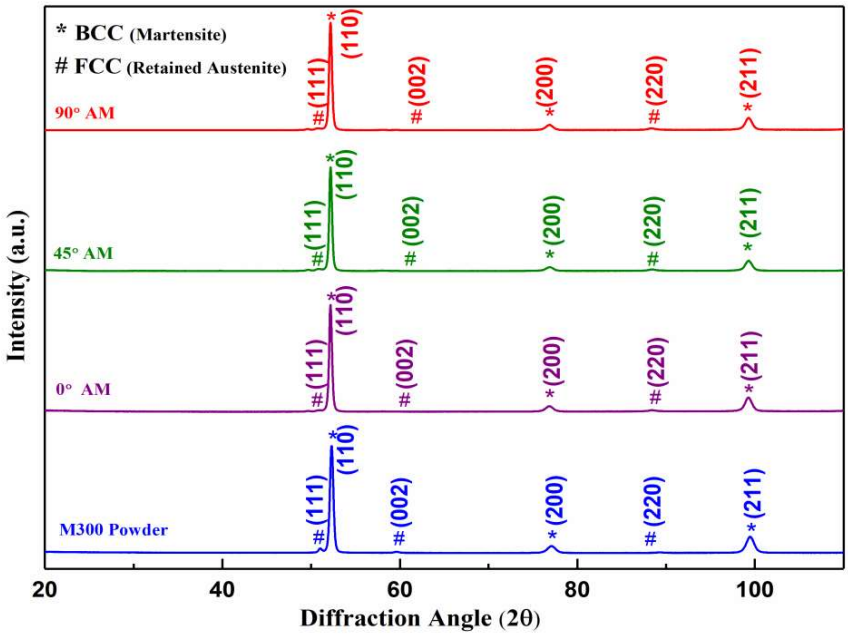

Fig. 3.6 X-Ray diffraction pattern of powder (M300) and AB samples built in different orientations revealing martensite (*bcc*) and a small fraction of austenite (*fcc*).

Bright field TEM micrographs of as-built AM samples in Fig. 3.7 (a) and (b) reveal parallel columnar grains with average width of 0.27 µm and cellular grains with average diameter of 0.38 µm. High density of dislocations was observed at grain boundaries due to very fast cooling rate during solidification. Nanocrystalline nature of the matrix can be confirmed from the diffraction rings depicted in the SAD pattern in Fig. 3.7(c) which can be indexed as bcc martensite phase. In addition to this, small needle-type precipitates (indicated by yellow arrow) and globular-type precipitates (indicated by red arrow) can be observed as shown in Fig. 3.8, due to intrinsic heat treatment which might have caused precipitation similar to that reported by C. Tan et al. [123].

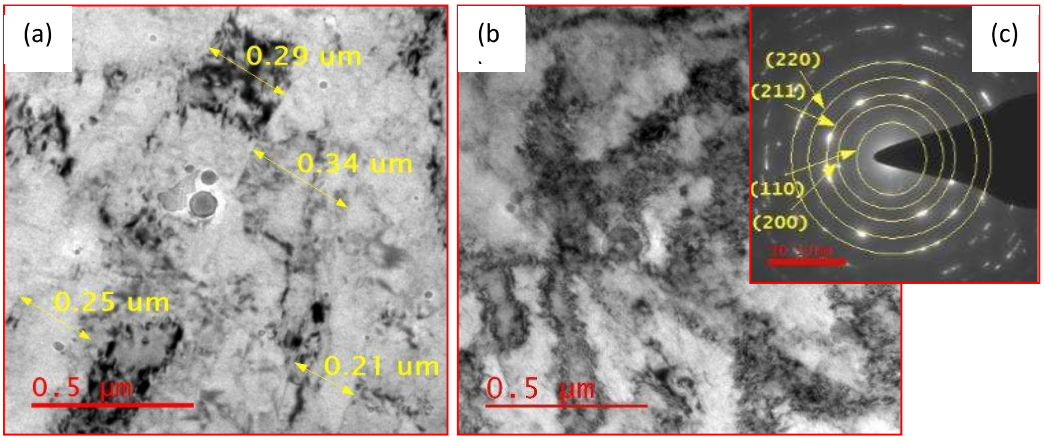

Fig.3.7 TEM bright field micrographs of 0^0 AB sample of M300 showing: (a) columnar grains (b) cellular grains and (c) corresponding SAD pattern.

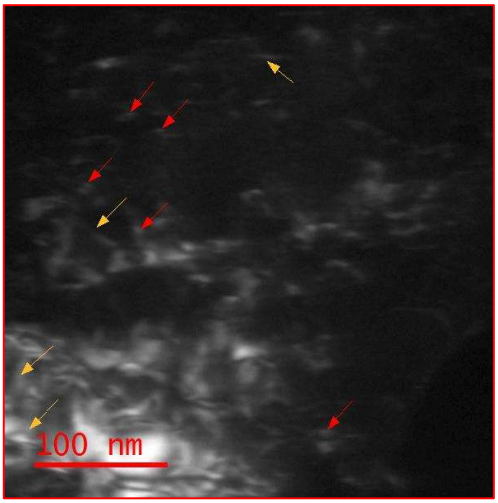

Fig. 3.8 Dark field micrograph of 45° AB sample of M300 showing triggered precipitation (as shown by arrows) due to intrinsic heat treatment.

3.3.2 Microstructure of heat-treated AB and CM samples

As-built samples and conventional samples were subjected to solution treatment (ST) at 815°C for 1 hour followed by air cooling and ageing (HT) at 520°C for 5 hours followed by air cooling to see the effect on heat treatment on microstructure. Only few partial melts pool boundaries can be seen after heat treatment. Lath type of martensite is observed in all orientations of AM-HT samples as shown in Fig. 3.9 (a). Martensitic laths are also observed in CM-HT sample as shown in Fig. 3.9 (b).

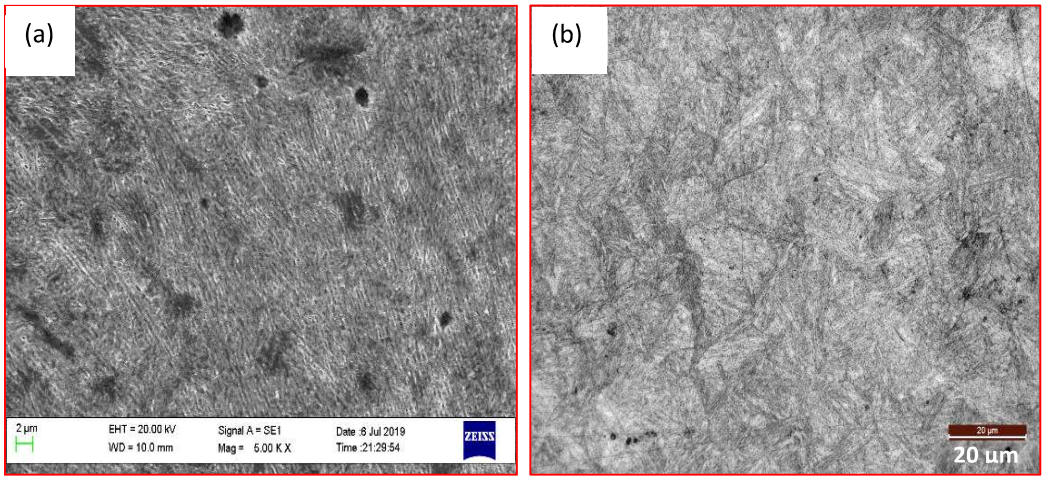

Fig. 3.9 Optical micrographs of heat-treated samples of M300 showing lath martensite in (a) transverse section of 0° HT sample and (b) CM-HT sample.

The x-ray diffraction analysis of HT samples is given in Fig. 3.10, which shows the presence of two phases, martensite (bcc) and reverted austenite (fcc). The percentage of reverted austenite was found to be 4% in CM-HT condition. As-built samples after heat treatment (AM-HT) were found to have higher percentage of reverted austenite i.e.7%, 9% and 12% in 0°, 90° and 45° orientations respectively as given in Table 3.2.

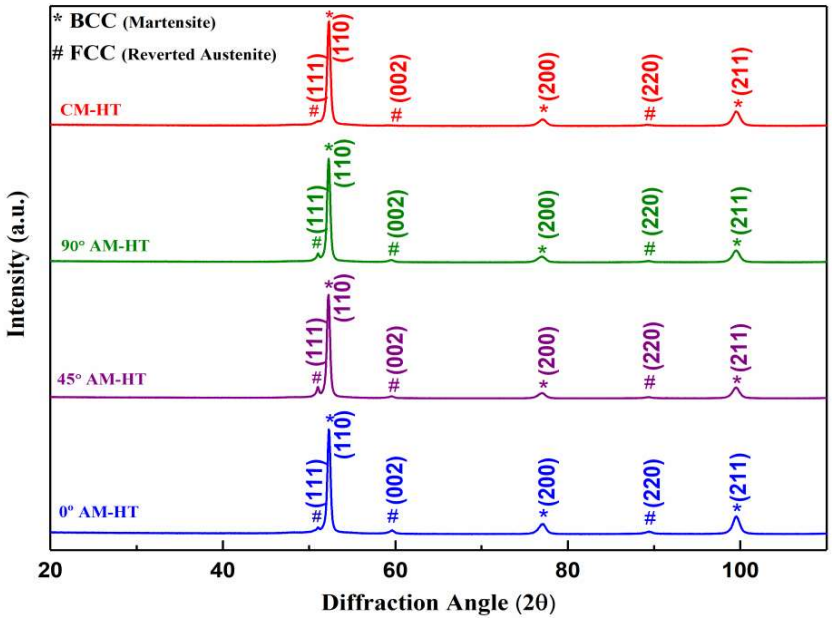

Fig. 3.10 X-Ray Diffraction patterns of CM-HT and AM-HT samples built in different orientations revealing martensite (*bcc*) and reverted austenite (*fcc*).

Table 3.2. Volume fraction of phases in AM and AM-HT samples in different orientations.

Orientation	Retained Austenite (%) in AB/CM samples	Reverted Austenite (%) In HT samples
0° AM	2	7
45° AM	3	12
90° AM	2	9
CM	2	4

Lath martensite is too fine to be seen by optical microscopy. Nanocrystalline nature of the matrix can be confirmed from the diffraction rings depicted in Figs. 3.12 and 3.13, which can be indexed as *bcc* martensite phase. The presence of reverted austenite is further confirmed by TEM. Bright field micrograph of AM-HT sample in 0° orientation along with SAD pattern shown in Fig. 3.11, confirms the presence of martensite (*bcc* phase) along with reverted austenite (*fcc* phase). Needle and globular precipitates were

also observed. It was confirmed by SAD that needle precipitates are Ni_3Ti and globular precipitates are Fe_2Mo as shown in Figs. 3.12 and 3.13.

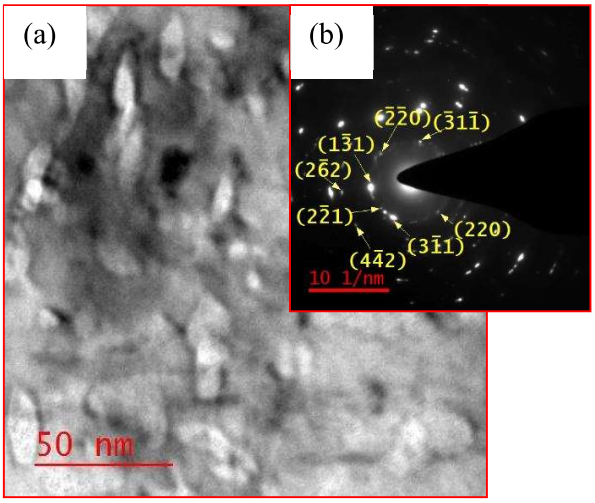

Fig. 3.11 Microstructure of M300 in 0^0AM-HT condition: (a) TEM Bright field micrograph showing reverted austenite and (b) SAD pattern revealing austenite (fcc phase, a=2.07 A°), beam direction (B), z: [-114]

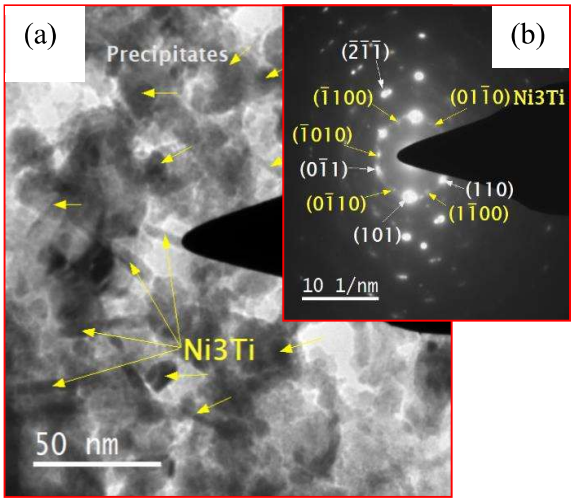

Fig 3.12 Microstructure of M300 in 45^0AM-HT condition:(a) TEM Bright field micrograph showing Ni_3Ti precipitates and (b) SAD pattern revealing Ni_3Ti (hcp phase, a=2.02 A^0 c=8.29 A^0), beam direction (B) z: [0001]

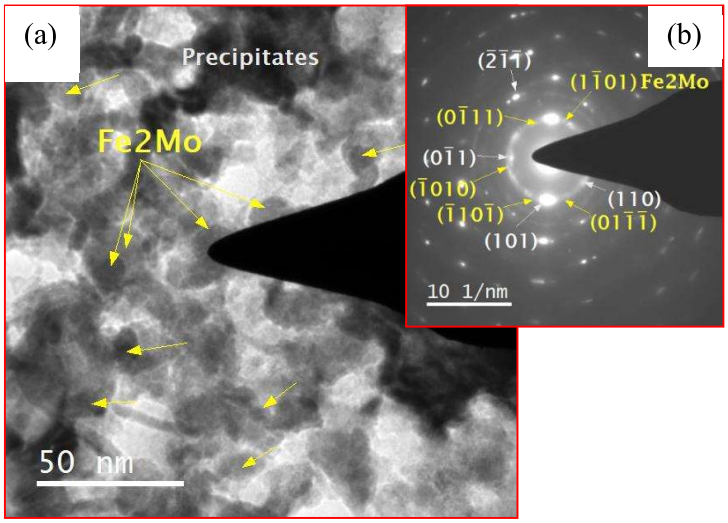

Fig. 3.13 Microstructure of M300 in 45^0AM-HT condition: (a) TEM Bright field micrograph showing Fe_2Mo precipitates (b) SAD pattern revealing Fe_2Mo (hcp phase, a=4.75 A^0 and c=7.76 A^0), beam direction (B) z: [1-21-3]

3.4 DISCUSSION

3.4.1 Characterization of Powder

In gas atomization, a stream of metal in molten state is disintegrated into droplets by jet of gas that results in almost spherical shape of the powder. The required size of powders needed for AM can be segregated by sieving [124]. For SLM, powder particles of size within the range of 15-50µm are preferred. In this investigation, average powder particle size of 25 µm was taken for processing by AM. The dendritic structure of the powder revealed is due to the high cooling rate in atomization which reaches to the order of 10^5 K/s. A small amount of retained austenite observed in XRD analysis might be due to incomplete transformation of austenite to martensite during atomization which is consistent with that reported in earlier work [125].

3.4.2 Relative density and surface roughness

Density is an important factor which influences the performance of AM parts [126]. Although higher energy density is preferred to get higher relative density, increase in

energy density above critical limits is found to cause a reduction in relative density [127, 71]. In order to examine the effect of process parameters and build rate (15 cm^3/h) on density and surface roughness, measurements of density and the surface roughness (R_a, R_q, R_z) of plates (in 0^o, 45^o and 90^o) were undertaken. The measurements show that there was no significant variation in density with change in build orientation indicating good inter and intra-layer metallurgical bonding between laser tracks.

On analyzing the surface roughness of as-built plates (0^o, 45^o and 90^o), it was found that in plates built in 0^o orientation, the surface roughness was due to hatching style i.e. strip pattern and in plates of 90^o as built orientation, the roughness was due to layering effect. Higher surface roughness was found in sample built in 45^o orientation on account of stair-step effect formed on layers. Each successive top layer are shifted laterally to get the desired orientation which results in stair-step effect on the surface generated which is commonly observed in this orientation [70].

3.4.3 Microstructural Characterization

In SLM, high cooling rates are observed on the boundaries of melt pool which promote segregation at boundaries resulting in laser tracks and melt pool boundaries being visible at low magnifications. OM and SEM after etching revealed laser tracks and melt pool boundaries in the present work which is similar to that observed in previous work [72]. Defects visible in 45^o and 90^o orientations might be due to un-melted powder, solidification shrinkage and entrapped gases as reported earlier [128]. In SLM, because of the extremely high cooling rate (10^5-10^7) K/s, formation of secondary dendrites gets suppressed which results in fine cellular and columnar microstructure which can be observed upon angle of view in melt pool [64]. The red dotted lines show grains boundary regions which confirm the columnar and cellular structure in regions marked as 1, and 2 in Fig 3.5(b). Fine grains are mainly observed but at some locations, coarse grains can

also be observed due to complex and non-uniform thermal gradients and thermal conduction [70]. During the processing of powder layer by layer with selected hatching pattern, the solidified layer gets exposed to cyclic reheating and gradual cooling, due to this intrinsic heat treatment (IHT), tiny precipitates were triggered in as-built SLM samples in all orientations, similar to the results earlier [129].

The microstructure of AM maraging steel is found to be martensitic with *bcc* structure. As maraging steel has very low carbon content and has high amounts of alloying elements such as Ni, Co, Mo, Ti as compared to that of plain carbon steel, AM maraging steel has *bcc* structure, and is confirmed by X-Ray diffraction. The retained austenite found in XRD analysis might be because of incomplete transformation of austenite to martensite during SLM processing and segregation of solute elements (mainly Ni) at cellular boundaries during solidification, as reported [130]. With the change in build orientation of SLM specimen, the heat transfer rate from the specimens to the base plate vary which results in different amounts of retained austenite due to incomplete transformation of austenite to martensite.

The AM samples during processing undergo complex heating and cooling cycles. The heat transfer rate in different oriented samples depends on the extent of contact area with the base plate and surrounding un-melted powder. After AM processing, the volume fraction of partial melt pool boundaries was higher in 45^{o} oriented samples (Fig.3.3) as compared to the boundaries in other build orientations. After heat treatment, austenite reversion takes place as austenite stabilizers diffuse towards these boundaries and provide more nucleation sites and larger amount of reverted austenite. After AM processing, the volume fraction of partial melt pool boundaries was higher (Fig.3.3) as compared to the boundaries in other build orientations. After heat treatment, austenite reversion takes place as austenite stabilizers diffuse towards these boundaries and cause

larger amount of reverted austenite. The presence of lath martensite with thick boundaries along with the austenite phase might be because of the reversion of martensite to austenite due to overaging treatment similar to that already observed [131]. While heating, austenite finish temperature is about 750^{o}C and upon cooling martensite start (Ms) and finish temperatures (M_f) are 164 ^{o}C and 61 ^{o}C, respectively in 18% maraging steel [132]. Solution treatment was given to the material by heating above austenite finish temperature and holding for about 1 hour followed by cooling to room temperature in air. Alloying elements get homogeneously dissolved in the austenite phase and further upon air cooling, supersaturated solid solution of martensite is obtained. In the present investigation, as-built specimens were given solution treatment at 815 ^{o}C for 1h which resulted in the conversion of retained austenite and martensite into homogenized austenite. Further, upon air cooling, only martensite was obtained in line with that reported in the literature [78, 67]. Aging was done at 520 ^{o}C for 5 hours followed by air cooling. It is reported that aging temperature higher than 500 ^{o}C and prolonged aging time promotes the reversion of martensite to austenite. The AM samples during processing undergo complex heating and cooling cycles. The heat transfer rate in different oriented samples depends on the extent of contact area with the base plate and surrounding un-melted powder. After AM processing, the volume fraction of partial melt pool boundaries was higher (Fig.3.3) as compared to the boundaries in other build orientations. After heat treatment, austenite reversion takes place as austenite stabilizers diffuse towards these boundaries and cause larger amount of reverted austenite. At high temperature and prolong aging, Ni release into Fe matrix that accompanies the transformation of Ni_3Ti to Fe_2Mo which is very stable precipitate and promotes the reversion of austenite [133].

In the current investigation, the aging condition studied falls in the overaging range of maraging steel which might have resulted in reverted austenite as revealed by XRD analysis [134].

3.5 CHAPTER SUMMARY

M300 grade maraging steel was processed by SLM with optimized processing parameters in different orientations. The microstructure and physical properties of the as-built and heat-treated specimens were systematically analysed. The following conclusions can be drawn from the present chapter:

1. Almost fully dense (>99.6%) M300 maraging steel plates were prepared by using selective laser melting in three orientations namely 0^o, 45^o and 90^o with laser energy density of 62.5 J/mm^3. Due to stair-step effect, plates built in 45^o orientation had highest surface roughness.

2. Fine grains (~0.31μm) and equiaxed grains (~2μm) were observed in as-built AM and as-received CM samples respectively. After heat treatment, lath martensite was observed in both AM and CM samples.

3. A small quantity of retained austenite (fcc phase) in martensitic matrix (bcc phase) was observed before heat treatment in both AM and CM samples. After aging due to austenite reversion, more amount of austenite (fcc phase) was detected along with the martensite.

4. Aging treatment led to precipitation of massive and homogeneously distributed needle-shaped nanosized precipitates of Ni_3Ti and also globular precipitates of Fe_2Mo in the martensitic matrix.